Landsat-Based Random Forest Analysis of LULC Dynamics and Urban Expansion in Sargodha, Pakistan (2000–2024)

Syed Fahad Hassan[1], Summaira Kousar[2], Amna Aslam[2], Hafiza Tayyaba Fayyaz[1], Rukhsar Shahzadi[1], Hira Manzoor[1], Saif Ullah Akhter[1]
[1]Institute of Space Science, University of the Punjab, Lahore
[2]Institute of Geography, University of the Punjab, Lahore
*Correspondence: fahadhassan408@gmail.com

Citation | Hassan. S. F, Kousar. S, Aslam. A, Fayyaz. H. T, Shahzadi. R, Manzoor. H, Akhter. S. U, "Landsat-Based Random Forest Analysis of LULC Dynamics and Urban Expansion in Sargodha, Pakistan (2000–2024)", IJIST, Vol. 08 Issue. 07 pp 3113-3131, September 2026
Received | Sep 09, 2026 **Revised |** Sep 25, 2026 **Accepted |** Sep 27, 2026 **Published |** Sep 30, 2026.

Urban growth in agriculturally productive districts creates a land-allocation challenge that is difficult to quantify without spatially consistent observations. This study investigates the magnitude, timing, and spatial expression of built-up expansion and associated cropland contraction in Sargodha District, Punjab, Pakistan, from 2000 to 2024. Six Landsat-based land-use/land-cover classifications (2000, 2005, 2010, 2015, 2020 and 2024), produced using Random Forest and post-classification comparison, were examined for four mapped classes: cropland, barren land, water and urban/built-up land. Built-up land increased from 290.22 to 391.92 km², a net gain of 101.70 km² (35.04% relative growth). Cropland declined from 5,319.22 to 5,239.88 km², a net reduction of 79.34 km². The greatest five-year urban gain occurred in 2010-2015 (39.69 km²), while spatial change maps identify urban-fringe expansion around Sargodha City and secondary centres. Barren land contracted by 22.19 km² and mapped water changed by only -0.17 km². Reported overall classification accuracies ranged from 89.00% to 95.95%, with Kappa values of 0.852-0.946. These results document a persistent agro-urban transition rather than a uniform loss of the district's agricultural landscape. The analysis provides a locally relevant baseline for monitoring peri-urban land conversion and prioritizing agricultural land protection. Interpretation remains conditional on the 30 m spatial resolution and the available time-specific validation information.

Keywords: Urban expansion; Cropland conversion; Random Forest; Landsat; Sargodha District.

Introduction:

Agricultural districts are increasingly required to accommodate housing, transport infrastructure and industrial activity without compromising the land base used for food production. In such settings, urban development is not simply a change in the number of buildings: it is a reorganization of the surface through which cropland, exposed soil, water and constructed features compete for a fixed area. Land-use/land-cover (LULC) mapping makes that reorganization visible by translating observations of the Earth's surface into spatially explicit classes. Long-running satellite archives are particularly useful because they permit comparisons before and after changes in local development intensity [1][2]. At the wider scale, the conversion of rural and natural landscapes into urban surfaces is recognized as a major source of landscape transformation and a challenge for sustainable regional planning [3][4].

The relationship between urban expansion and agricultural land is especially important in Punjab, Pakistan. Much of the province's settlement network is embedded in irrigated agricultural plains. Urban growth therefore frequently extends from an established city into cultivation at its periphery, rather than into large areas of unproductive land. Evidence from Rawalpindi, Khanewal and Multan has illustrated this intersection between urban growth, land conversion and surface-environment changes, although the spatial scales and classification designs vary among studies [5][6][7][8]. Recent geospatial investigations published in the International Journal of Innovations in Science & Technology also document urban growth and agricultural displacement in Lahore and Khairpur [9][10]. The comparisons establish the regional significance of the process; they do not substitute for an independent district-scale estimate for Sargodha.

Sargodha District provides a distinct case because intensive cropland remains the dominant mapped land cover while urban growth occurs around Sargodha City and several smaller centres. The district supports agricultural production, including wheat and citrus, alongside residential, educational, commercial and industrial activities. Expansion of the built environment may fragment parcels, increase competition for roadside plots and create longer-term pressure on cultivated land. Yet the extent of urban growth cannot be inferred reliably from demographic change or individual local development schemes alone [11]. A sequence of comparable satellite classifications is needed to separate persistent district-wide changes from the variation associated with land preparation, seasonal fallowing and image-acquisition conditions [12][13][14].

The Landsat programme offers multi-decadal multispectral imagery at 30 m spatial resolution, which is appropriate for reconstructing broad land-cover trends across a district. Its value derives from relatively consistent imaging, repeated acquisition and an open archive [1]. However, the spectral separation of built-up surfaces from dry bare soil can be difficult in agricultural plains. Similar reflectance patterns may cause an apparent change to be confused with a temporarily uncultivated field. Vegetation, built-up and water indices can help discrimination, but they do not eliminate errors caused by mixed pixels or variation in crop stage [12][15]. These challenges strengthen the case for supervised classification that accommodates multiple predictor variables and for explicit accuracy assessment [16][17][18].

Random Forest (RF) provides a practical method for such applications. By combining decision trees fitted to different subsets of training information, RF can describe nonlinear relationships between spectral characteristics and thematic classes without requiring a single parametric distribution [19]. The algorithm has been used extensively for land-cover and agricultural mapping, although its performance depends on the reference labels, temporal consistency and validation design [20][21]. Once images for separate years are classified using the same class definitions, post-classification comparison enables both the net change of each class and the spatial distribution of class transitions to be examined. Change mapping must

nevertheless be interpreted with caution because errors in the classifications from two dates may be carried forward into change estimates [16][22].

Prior work in Pakistan has examined urban growth in major metropolitan areas and the thermal or ecological consequences of land conversion [6][7][8][9][10][23][24][25]. For Sargodha, the more immediate question is how a predominantly agricultural district has accommodated built-up expansion over the past two decades, and whether the pace of that expansion has been constant. A locally focused analysis is valuable because the magnitude of urban land growth and its relationship to cropland cannot be assumed to match those of Lahore or Multan. A six-date comparison also reveals whether short intervals dominate the long-term change, information that is obscured when only the beginning and ending years are considered.

Research Gap:

Although previous Landsat-based studies in Pakistan have examined urban expansion and LULC change in locations such as Rawalpindi, Khanewal, Multan, Lahore and Khairpur, the reviewed literature does not provide the same six-epoch, district-wide assessment for Sargodha over 2000–2024. In particular, the temporal distribution of built-up gains and their relationship with cropland contraction have not been consolidated here using a consistent four-class scheme and interval-wise comparison.

This study addresses one closely defined objective: to quantify and describe the temporal and spatial growth of built-up land and the concurrent transformation of cropland in Sargodha District between 2000 and 2024. The principal contribution is a consolidated account of change magnitude, five interval-specific rates, spatial concentration and classification reliability using the original Landsat-derived results. Barren land and water are included only as contextual classes needed to maintain the district-wide land balance. The article does not attempt to predict future land cover, model population as a causal driver or estimate crop yield or economic loss. These outcomes require independent data and methods not included in the current analysis.

Research Objectives and Hypothesis:

- To classify and validate cropland, barren land, water bodies and built-up areas in Sargodha District for six Landsat observation years using the Random Forest algorithm.
- To quantify net land-cover changes across successive periods and assess the spatial pattern of urban expansion and cropland reduction during 2000-2024.

Hypothesis:

Built-up land expanded and cropland declined during 2000-2024, with the most visible changes around Sargodha City and adjoining towns.

Novelty and Analytical Focus:

Unlike a general catalogue of every surface process in the district, the present assessment links six classified epochs to the specific problem of built-up growth on an agricultural landscape. It combines class area accounting, interval-wise net changes, spatial transition maps and an explicit review of reported map accuracy. The central distinction is between observable land-cover change and a proposed explanation for that change: conversion patterns are estimated from satellite classifications, while demographic, infrastructural and policy explanations are discussed as plausible drivers rather than quantified causal effects.

Study Novelty and Contribution:

The contribution is not the use of Landsat or Random Forest alone, both of which are established methods. Rather, it is the Sargodha-specific comparison of six observation years (2000, 2005, 2010, 2015, 2020 and 2024), combined with consistent four-class mapping, five interval-specific change estimates, spatial transition visualization and class-wise accuracy

reporting. This provides a district-scale baseline that complements, rather than duplicates, earlier Pakistan studies focused on other locations or different analytical outcomes.

Materials and Methods:

Study Area and Analytical Boundary:

Sargodha District lies in Punjab Province, Pakistan, within an irrigated alluvial landscape associated with the Jhelum and Chenab River systems. It includes Sargodha City and agricultural settlements such as Bhalwal and Shahpur. The district experiences a semi-arid climate with hot summers and comparatively mild winters. Wheat, citrus and other crops occupy large parts of the surrounding plains, and canal-fed agriculture is important to local livelihoods. These conditions make the urban–cropland boundary a relevant indicator of competing land demands. The study-area map shows the district's position in Pakistan and Punjab, its hydrological setting and major transport connections (Figure 1).

The approximate administrative area of the district is 5,864 km². However, the four mapped classes in each year of the original results sum to 5,794.49 km². Percentages and net changes are therefore calculated using the 5,794.49 km² mapped footprint indicated by the class-area table, rather than the approximate administrative total. The 69.51 km² difference between reported areas requires reconciliation against the original GIS boundary and pixel accounting. It does not change the arithmetic difference between the class areas reported for the six epochs.

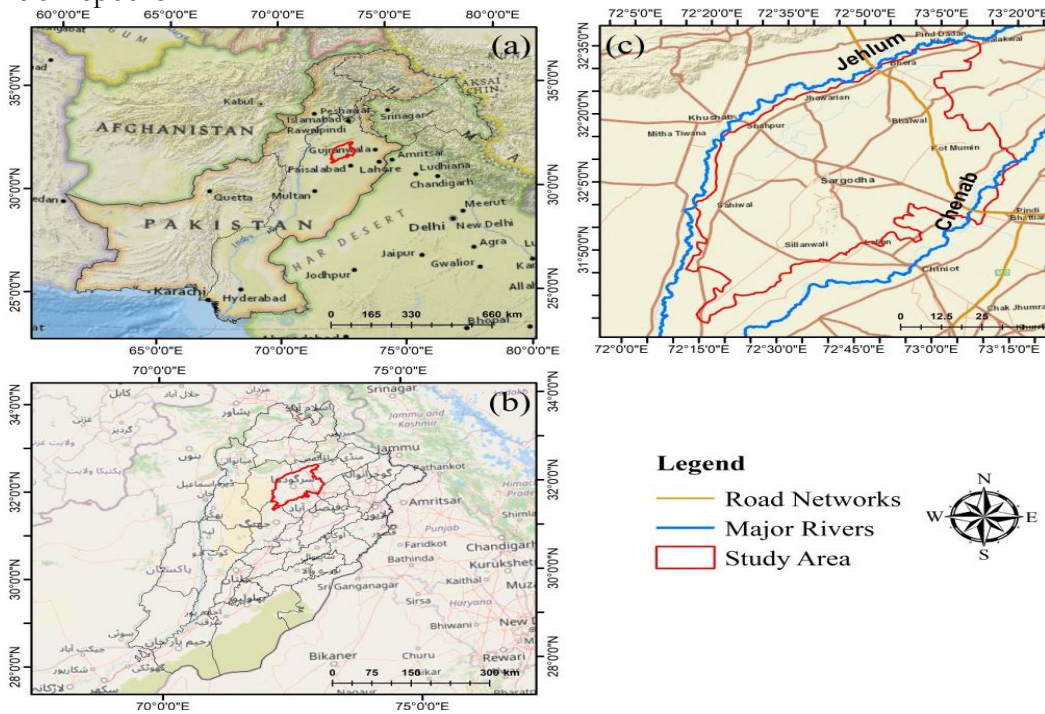


Figure 1. Location map of Sargodha District, Punjab, Pakistan, showing (a) its geographical location within Pakistan, (b) its position within Punjab Province, and (c) the detailed study area boundary with major rivers and road networks.

Satellite Data and Reference Information:

The analysis uses six classified years: 2000, 2005, 2010, 2015, 2020 and 2024. The satellite archive comprised Landsat 5 TM, Landsat 7 ETM+, Landsat 8 OLI and Landsat 9 OLI-2 imagery acquired from the USGS Earth Explorer archive. Reflectance bands in the visible, near-infrared (NIR) and short-wave infrared (SWIR) regions provided the spectral basis for interpretation. All datasets were analyzed at 30 m nominal spatial resolution. The image-selection procedure prioritized relatively cloud-free observations from February to March in order to limit differences caused by seasonal crop conditions. Ancillary road,

drainage, administrative boundary and historical high-resolution image layers complemented the Landsat data [1][26].

The documented classification design comprised 200 training polygons, with 50 representing each of the four classes. Training-site labels were informed by historical high-resolution imagery, false-colour composites and field knowledge. A separate dataset of 150 GPS reference points was reported from observations during 2023-2024. A complete year-wise inventory of independent historical reference labels was not available in the methodological records. The earlier-year accuracy scores are reproduced without assuming that all epochs had equivalent independent ground-reference information. This distinction matters because present-day GPS observations cannot by themselves establish the true class at a particular location in 2000 or 2005 [16][22].

Image Preparation and Classification Features:

The processing description combines terrain-corrected Landsat data, radiometric calibration, image co-registration, cloud screening and clipping to the study boundary. It refers to Top-of-Atmosphere reflectance conversion and to image preparation in Google Earth Engine, ArcGIS and Python. These steps were intended to make the spectral observations suitable for comparison across acquisition dates. The documented workflow proceeds from data acquisition and preprocessing to feature calculation, supervised classification, accuracy assessment and post-classification change estimation (Figure 2). Scene acquisition dates, product identifiers, mask configurations and a full processing script were not available for independent reproduction [26].

A four-category classification scheme was used throughout the reported results: cropland, barren land, water and urban/built-up land. Cropland covers managed agricultural surfaces, including seasonal crops and cultivated orchards. Barren land represents exposed, uncultivated or fallow surfaces. The urban class groups settlements, built infrastructure, roads and related impervious or developed features. Water covers rivers, canals, ponds and other visible water surfaces. In this scheme, urban area is a remotely sensed class rather than a formal municipal boundary, and barren land may include temporarily bare agricultural fields. These definitions are crucial when interpreting the net class changes.

The classification feature set includes the six principal reflective bands together with the Normalized Difference Vegetation Index (NDVI), Normalized Difference Built-up Index (NDBI) and Modified Normalized Difference Water Index (MNDWI). NDVI compares NIR and red reflectance and is used to distinguish photosynthetically active vegetation from many non-vegetated surfaces. NDBI compares SWIR and NIR reflectance to support identification of built-up surfaces [27]. MNDWI compares green and SWIR reflectance to enhance water features and suppress competing land signals [28]. In the notation of this study, with reflectance values ϱ, these indices are: $NDVI = (\varrho NIR - \varrho Red)/(\varrho NIR + \varrho Red)$; $NDBI = (\varrho SWIR - \varrho NIR)/(\varrho SWIR + \varrho NIR)$; and $MNDWI = (\varrho Green - \varrho SWIR)/(\varrho Green + \varrho SWIR)$. The recorded predictor table specifies MNDWI; this study therefore follows that definition rather than assuming an additional water index.

Random Forest Classification and Quality Assessment:

The supervised per-pixel classification used RF in a Python scikit-learn workflow supported by GIS operations. The multiband spectral information and indices formed the candidate predictor set. Each classified pixel was assigned a single LULC category. A 3 × 3 majority filter was reported as a post-classification operation to suppress isolated pixels. RF was selected for its ability to integrate correlated reflectance and index information, although the model's number of trees, tree depth, feature-sampling settings and random-state configuration were not documented in the available processing record. No additional hyperparameter values are assumed in this paper [19][20].

Algorithm 1. Random Forest-based LULC classification and change analysis

Input: Preprocessed Landsat spectral bands; NDVI, NDBI and MNDWI layers; labelled training samples; independent reference samples; six target years (2000, 2005, 2010, 2015, 2020 and 2024).
Output: Four-class LULC maps, accuracy statistics and interval-wise LULC change estimates.
1. For each target year, acquire and preprocess the corresponding Landsat imagery, including cloud screening, radiometric preparation, co-registration and clipping to the study boundary.
2. Generate a predictor stack by combining the available reflective bands with NDVI, NDBI and MNDWI.
3. Extract predictor values at the labelled training-sample locations and associate each sample with one of four classes: cropland, barren land, water or urban/built-up.
4. Train a Random Forest classifier on the labelled samples. Use the model configuration applied in the original analysis; record the number of trees and maximum tree depth from the original software settings rather than estimating these values retrospectively.
5. Apply the trained classifier to the predictor stack to assign each image pixel to one of the four LULC classes and generate the classified map for that year.
6. Apply the reported 3 × 3 majority filter to reduce isolated classified pixels.
7. Compare the classified map with the available reference samples and derive the confusion matrix, overall accuracy, user's accuracy, producer's accuracy and Kappa coefficient.
8. Repeat Steps 1–7 for all six observation years using the same class definitions and predictor framework.
9. Perform post-classification comparison between successive maps; calculate class areas, net area changes and annualized interval changes for 2000–2005, 2005–2010, 2010–2015, 2015–2020 and 2020–2024.
10. Summarize the spatial distribution of mapped transitions and report the results with the corresponding accuracy information.

Computational Implementation:

The computational workflow was organised as a repeatable sequence of raster preparation, feature construction, supervised learning, map production, accuracy evaluation and temporal change accounting. The activities below describe the computer-based operations supported by the methods and results reported in this study. They do not imply that undocumented model settings or unavailable processing scripts have been reconstructed.

Data organization and raster preparation: Landsat scenes for 2000, 2005, 2010, 2015, 2020 and 2024 were organised by observation year. The reported preprocessing operations included radiometric preparation, cloud screening, co-registration and clipping to the Sargodha study boundary. Before stacking, the reflective bands and derived indices were required to share a common spatial reference, pixel alignment, extent and nominal 30 m resolution. No unreported scene identifiers, cloud-mask thresholds or resampling settings are assumed.

Spectral feature computation: For each year, the predictor stack was assembled from the six reflective bands and the NDVI, NDBI and MNDWI layers. The index calculations used the equations already specified in the manuscript. To avoid undefined values in computer processing, pixels for which an index denominator equals zero or is masked were retained as NoData and excluded from model fitting and prediction.

Training-data Extraction and Class Encoding:

Predictor values were sampled at the labelled training-polygon locations and paired with the four target labels: cropland, barren land, water and urban/built-up. The class labels were encoded consistently across all observation years. The separately reported reference observations were reserved for map evaluation and were not treated as additional training samples in the described workflow.

Random Forest Model Fitting and Pixel-wise Inference:

A scikit-learn Random Forest classifier was fitted to the labelled predictor samples and then applied to the corresponding annual predictor stack. The trained estimator assigned one of the four LULC labels to each valid pixel. The number of trees, maximum tree depth, feature-sampling rule, random seed and any class-balancing settings must be taken from the original Python configuration; they are intentionally not specified here because the available processing record does not provide them.

Post-classification filtering and map export:

The classified raster for each year was processed using the reported 3 × 3 majority filter to reduce isolated single-pixel assignments. The resulting maps were retained with a common class code scheme so that corresponding categories could be compared across dates. Filtering was applied as a cartographic post-processing step and does not replace independent accuracy assessment.

Accuracy Computation:

For each available year-specific reference set, the classified labels were compared with the reference labels to construct a confusion matrix. Overall accuracy was computed as the sum of the diagonal counts divided by the total number of evaluated samples. User's accuracy for a mapped class was computed as its correctly mapped count divided by the row total for that mapped class; producer's accuracy was computed as the correctly mapped count divided by the column total for the corresponding reference class. Kappa was retained as the agreement statistic reported in the original results. These calculations require the reference-sample design and class ordering to be documented consistently.

Area and Temporal-change Computation:

For each class and observation year, the mapped area was derived from the number of classified pixels multiplied by the area represented by one valid pixel in the analysis coordinate system. Net change was calculated as $A(t2) - A(t1)$, relative change as $100 \times [A(t2) - A(t1)]/A(t1)$, and mean annual net change as $[A(t2) - A(t1)]/(t2 - t1)$. Successive classified maps were also compared pixel by pixel to form transition counts between the four classes. Transition counts should be reported separately from net class-area differences.

Quality-control Checks and Outputs:

Before producing tables and figures, the computer workflow checked that all annual maps used the same class codes and spatial grid, that NoData pixels were excluded from area totals, and that the four class areas summed to the mapped footprint for each year. Outputs comprised the six classified LULC maps, confusion-matrix statistics, class-area summaries, interval-wise net-change tables and spatial transition layers. The manuscript reports a mapped footprint of 5,794.49 km² and separately notes that it differs from the approximate administrative area; this discrepancy remains a data-boundary issue requiring verification against the original GIS files.

Algorithm 2. Computer-based implementation sequence for annual LULC mapping and change analysis

Input: Annual Landsat predictor bands; NDVI, NDBI and MNDWI; labelled training samples; available independent reference samples; study boundary; six target years.
For each target year y in {2000, 2005, 2010, 2015, 2020, 2024}:
Prepare and align the cloud-screened Landsat bands to the common study grid.
Calculate NDVI, NDBI and MNDWI; mask invalid or NoData pixels.
Stack reflective bands and indices into the annual predictor image X_y.
Extract X_y at labelled training locations and associate the four LULC class labels.
Fit the Random Forest estimator using the original, documented model configuration.
Predict the class label for every valid pixel in X_y to produce map M_y.
Apply the reported 3 × 3 majority filter and save M_y with the common class codes.
Compare M_y with the available independent reference labels and calculate the confusion matrix and accuracy statistics.
Count valid pixels by class and convert counts to area using the analysis-grid pixel area.
For each successive pair of maps (M_t1, M_t2): calculate class-area differences, relative changes, annualised changes and pixel-level transition counts; export tables and spatial change layers.
Output: Six comparable LULC maps, year-wise accuracy statistics, class-area tables, interval-wise change estimates and transition layers.

Classification accuracy was evaluated using confusion-matrix-derived user's accuracy (UA), producer's accuracy (PA), overall accuracy (OA) and the Kappa coefficient. UA expresses the fraction of a mapped class correctly represented among reference observations assigned to that map class; PA expresses the fraction of a reference class correctly identified by the classifier. OA is the total fraction of agreement across the confusion matrix. The Kappa coefficient is reproduced for comparability with the original work, but it is not treated as a substitute for class-wise error information or uncertainty in area estimates [16][22][29]. A current best-practice area assessment would additionally report sampling design, time-specific reference interpretation, adjusted area estimates and confidence intervals. These additional statistical outputs were not part of the available evaluation record.

Change Accounting and Spatial Interpretation:

For each class, mapped net change between times t1 and t2 was evaluated as $\Delta A = A(t2) - A(t1)$, where A is the mapped class area in square kilometres. Relative change is calculated as $100 \times \Delta A/A(t1)$; the change in the proportion of the mapped district is expressed separately in percentage points. The average annual net change is ΔA divided by the interval length in years. This distinction avoids confusing a percentage reduction in class area with a percentage-point reduction in land-cover share. Five intervals were retained: 2000-2005, 2005-2010, 2010-2015, 2015-2020 and 2020-2024.

Post-classification comparison of successive categorical maps provides the spatial basis for detecting persistence and class-to-class change [13][30]. A transition-flow diagram and multi-date transition maps were produced. These are used in the current article to identify broad locations and directions of change rather than to infer an exact contribution of cropland to new built-up land without a complete cross-tabulation matrix. Net cropland decline and net built-up increase can occur simultaneously without proving that every lost cropland pixel became urban land. Area totals and interval gains are taken directly from the numerical tables, while spatial descriptions derive from the change maps and transition graphics.

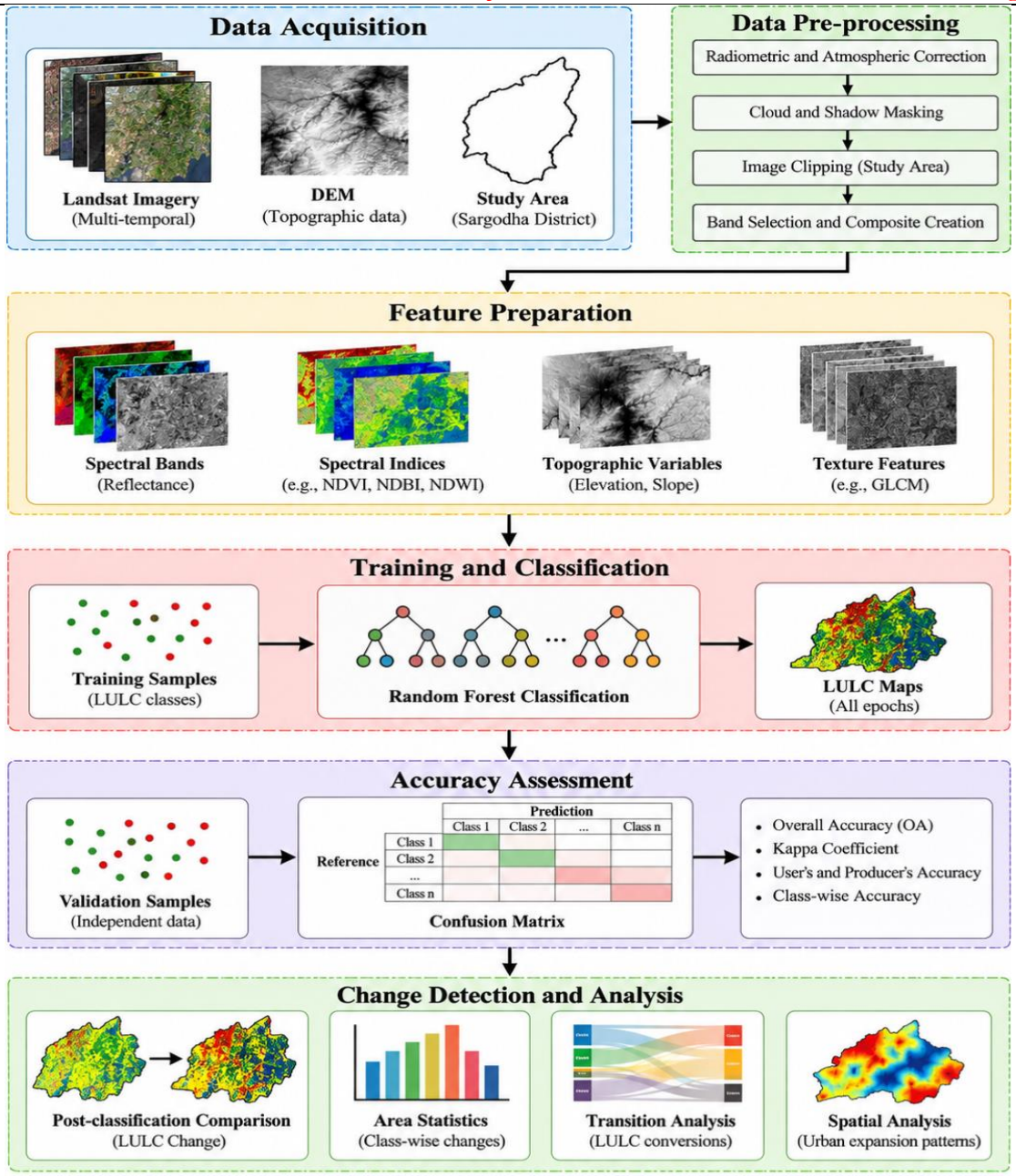


Figure 2. Satellite preprocessing, Random Forest classification, accuracy assessment and change-detection workflow.

Results:

Evolution of Built-up and Cropland cover:

The mapped district was dominated by cropland throughout the six-date observation series (Table 1). In 2000, cropland occupied 5,319.22 km² or 91.798% of the mapped area. By 2024 its extent had decreased to 5,239.88 km² or 90.429%. Thus, the absolute net reduction was 79.34 km². Expressed against the 2000 cropland baseline, the decline was 1.49%; expressed as a change in mapped-area share, it was 1.369 percentage points. This distinction avoids conflating the relative loss in cropland area with its change in district-wide percentage share.

Built-up land followed the opposite trajectory. The mapped urban class occupied 290.22 km² in 2000, increased to 297.71 km² in 2005 and reached 320.71 km² by 2010. It then grew to 360.40 km² in 2015, 372.62 km² in 2020 and 391.92 km² in 2024. Across 24 years,

urban land gained 101.70 km², or 35.04% relative to its 2000 extent. Its share of the mapped district increased from 5.009% to 6.764%, a change of 1.755 percentage points. Built-up area therefore expanded in every reported interval despite differences in the pace of expansion.

The contrast between these trajectories is important for understanding the district's development. The built-up gain was larger than the net Cropland decrease of 22.36 km². This difference corresponds closely to the combined declines in barren land and water (22.19 and 0.17 km², respectively), which is consistent with the conservation of area across the four classified classes. It is not proof that specific parcels followed one particular transition pathway. Rather, it establishes that the urban class increased within a closed four-class land-accounting system and that cropland was its largest declining counterpart in net terms.

Table 1. Class-wise LULC area statistics for Sargodha District, 2000-2024 (area in km²; share in %).

Year	Cropland	Barren land	Water	Urban/built-up
2000	5,319.220 (91.798)	154.450 (2.665)	30.600 (0.528)	290.220 (5.009)
2005	5,314.760 (91.721)	150.880 (2.604)	31.140 (0.537)	297.710 (5.138)
2010	5,291.120 (91.313)	150.360 (2.595)	32.300 (0.557)	320.710 (5.535)
2015	5,267.100 (90.898)	136.950 (2.363)	30.040 (0.518)	360.400 (6.220)
2020	5,255.680 (90.701)	134.270 (2.317)	31.920 (0.551)	372.620 (6.431)
2024	5,239.880 (90.429)	132.260 (2.283)	30.430 (0.525)	391.920 (6.764)

The multi-year land-cover maps (Figure 3) show continued agricultural dominance alongside a more visible constructed footprint around Sargodha City and other settlement concentrations. The mapped spatial pattern is not one of abrupt replacement of the entire agricultural landscape; it is characterized by localized expansion, infill and outward extension of existing built-up patches. The relative prominence of Sargodha City, Bhalwal and Shahpur is consistent across the interpreted maps. These observations provide geographical context for the numerical trends but are not accompanied by an urban-fringe buffer analysis or settlement-wise area breakdown in the available maps.

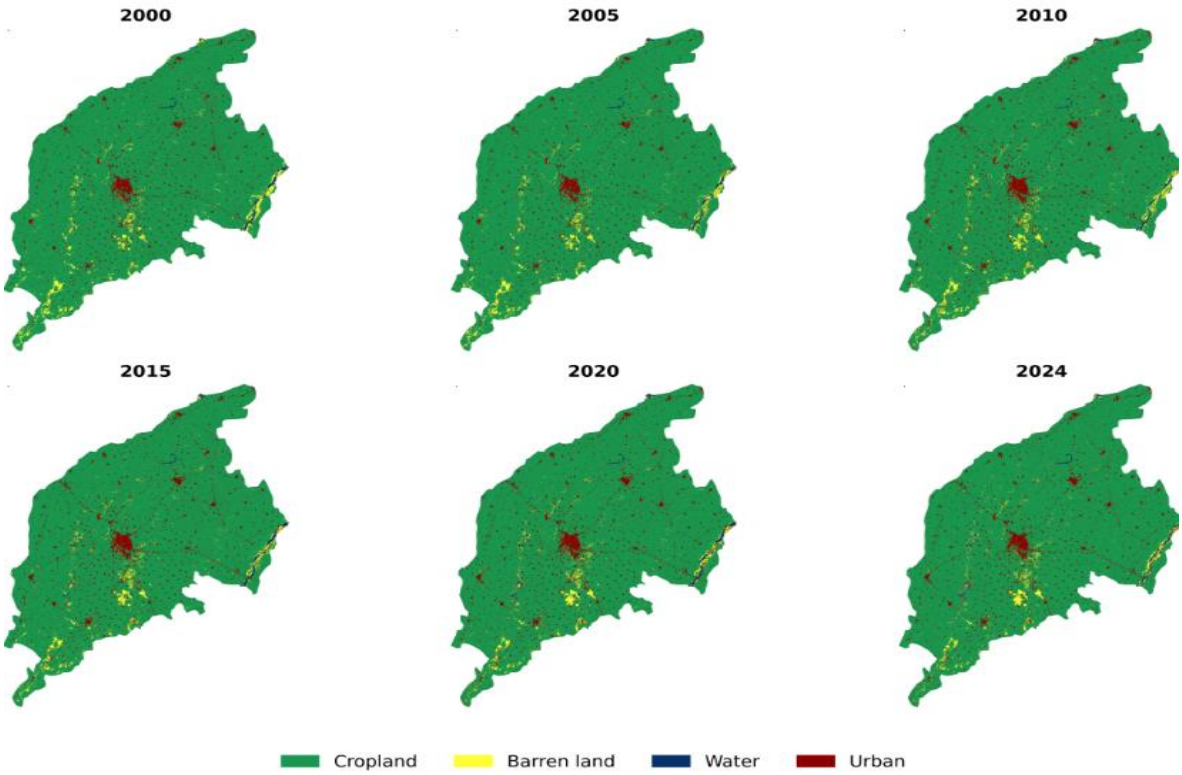


Figure 3. Classified cropland, barren land, water and urban land-cover maps, 2000-2024.

Timing and Rate of Built-Up Expansion:

The five inter-epoch changes show that urban expansion was not uniform (Table 2). The earliest interval, 2000-2005, recorded only 7.49 km² of net additional built-up land. The gain increased to 23.00 km² during 2005-2010 and peaked at 39.69 km² during 2010-2015. The following interval, 2015-2020, recorded 12.22 km², while 2020-2024 added a further 19.30 km². The 2010-2015 phase accounted for 39.03% of the district's entire 2000-2024 net built-up gain. Urban area increased by an average of 7.94 km² per year in that five-year phase, compared with 1.50 km² per year in 2000-2005.

During 2020-2024, the annual average net urban gain was 4.83 km², higher than the 2.44 km² per year of 2015-2020 but below the rate recorded in 2010-2015. Over the full observation window, the average was 4.24 km² per year. These rates are descriptive means based on the classified endpoints; they are not annual estimates for each intervening year. The chart of class areas (Figure 4) illustrates the continuous increase of the urban category, the gradual decline in cropland and the comparatively smaller magnitude of change in the two remaining categories.

Cropland losses also occurred in each of the five intervals, but their magnitude varied. The first five-year period lost 4.46 km². The losses during 2005-2010 and 2010-2015 were 23.64 and 24.02 km², respectively. Between 2015 and 2020, the cropland class contracted by 11.42 km²; in the final four-year interval it declined by 15.80 km². The periods of substantial cropland contraction overlap with the strongest observed built-up expansion, supporting the interpretation of competing urban and agricultural land demands at the district scale.

Table 2. Interval-wise and cumulative net class changes (km²), Sargodha District, 2000-2024.

Period	Cropland	Barren land	Water	Urban/built-up
2000–2005	−4.46	−3.57	+0.54	+7.49
2005–2010	−23.64	−0.52	+1.16	+23.00
2010–2015	−24.02	−13.41	−2.26	+39.69
2015–2020	−11.42	−2.68	+1.88	+12.22
2020–2024	−15.80	−2.01	−1.49	+19.30
Total, 2000–2024	−79.34	−22.19	−0.17	+101.70

Differences between mapped class areas are net changes, not gross class-to-class transition areas.

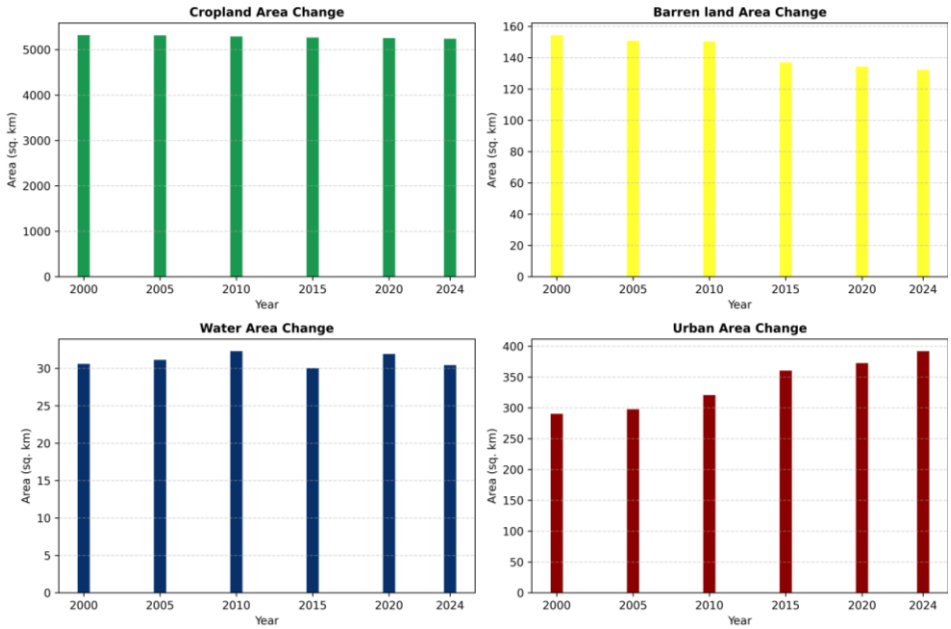


Figure 4. Changes in mapped LULC areas for the six observation years.

Contextual Changes in Barren Land and Water:

Barren land decreased from 154.45 km² in 2000 to 132.26 km² in 2024, a net reduction of 22.19 km² or 14.37% relative to its initial area. The greatest five-year decrease was recorded in 2010-2015 (13.41 km²). Because the barren category incorporates exposed and potentially fallow surfaces, its mapped contraction may reflect agricultural reclamation, the construction of built features, phenological conditions or a combination of these mechanisms. The transition graphics show barren-to-cropland movements, but the available numerical summaries do not establish how much of the long-term net barren loss reflects each cause.

Mapped water was a comparatively small category, ranging between 30.04 and 32.30 km² in the six observations. The earliest and final estimates were 30.60 and 30.43 km². Their difference of -0.17 km² is small relative to the mapped district extent. This supports a descriptive finding of limited net change in detectable water surfaces, not a claim that irrigation supply, hydrological functioning or groundwater conditions were stable. At Landsat resolution, canals, narrow watercourses and seasonally inundated areas may be difficult to classify consistently.

Classification Accuracy and Reliability:

Reported overall accuracy (OA) ranged from 89.000% in 2000 to 95.952% in 2024 (Table 3). Values for the intervening epochs were 93.006% in 2005, 91.360% in 2010, 94.046% in 2015 and 93.467% in 2020. Although the endpoint accuracy improved, the series was not monotonically increasing. Corresponding Kappa coefficients were 0.852, 0.906, 0.884, 0.920, 0.912 and 0.946. Thus, the highest reported OA and Kappa were obtained for 2024, while the lowest occurred for 2000.

Built-up user's accuracy increased from 88.889% in 2000 to 95.455% in 2024; built-up producer's accuracy rose from 90.435% to 96.250%. The cropland class also performed better in the final epoch than in the first, with user's accuracy rising from 90.435% to 96.414%. For barren land, the reported 2000 user's accuracy of 82.320% was lower than the corresponding value for built-up, indicating greater uncertainty in identifying exposed surfaces in the earliest classification. The water class had comparatively high user's accuracy throughout, ranging from 94.839% to 98.171%.

These results give useful information about the reliability of each snapshot. They do not, however, provide a confidence interval for the urban change estimate or an accuracy assessment specifically for transitions such as cropland-to-built-up. In particular, two individually accurate maps may still produce uncertain rare-class conversions when compared pixel by pixel. The reported accuracy statistics are therefore treated as evidence about thematic map agreement, not as direct evidence that every mapped conversion is correct or that a particular socioeconomic cause has been established.

Table 3. Classification accuracy of the four mapped LULC classes, 2000-2024 (percent except Kappa).

Year	Crop UA	Crop PA	Barren UA	Barren PA	Water UA	Water PA	Urban UA	Urban PA	OA	Kappa
2000	90.435	86.667	82.320	87.647	94.839	91.875	88.889	90.435	89.000	0.852
2005	93.902	94.286	89.888	91.429	96.795	91.515	91.915	93.913	93.006	0.906
2010	92.982	90.213	87.135	87.647	95.455	92.453	90.171	94.619	91.360	0.884
2015	95.161	95.161	90.556	93.143	97.452	92.727	93.277	94.468	94.046	0.920
2020	94.958	94.167	90.116	91.176	96.711	91.875	92.308	95.575	93.467	0.912
2024	96.414	96.800	93.989	95.556	98.171	94.706	95.455	96.250	95.952	0.946

Spatial Pattern of Conversion:

The transition-flow figure provides a complementary view of the movement between the four mapped categories (Figure 5). Its principal interpretive value in the focused article is to show that cropland is involved in built-up transitions while barren and cropland surfaces also exchange pixels in successive periods. The chart should not be interpreted as a validated estimate of the percentage of new urban land directly originating from cropland unless the underlying pixel-level transition matrix is supplied and checked. In particular, the net change table cannot on its own support a percentage attribution for the source of every newly urbanized pixel.

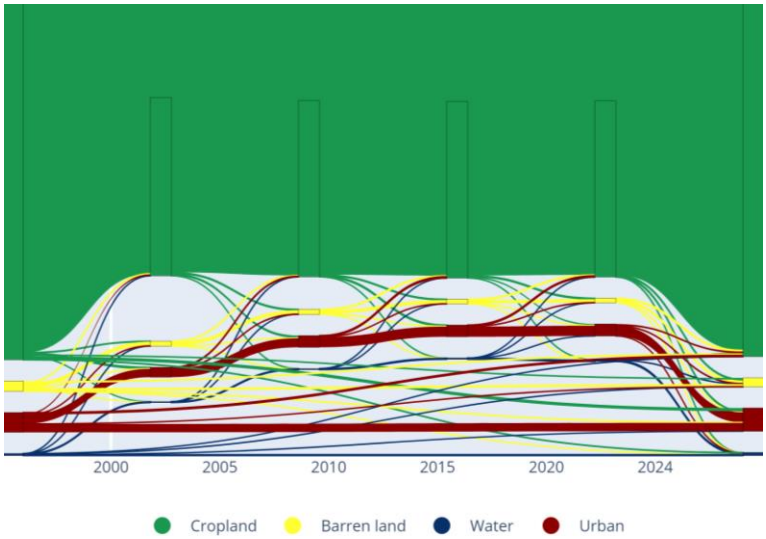


Figure 5. LULC transition flows (2000-2024) in Sargodha District, illustrating proportional changes.

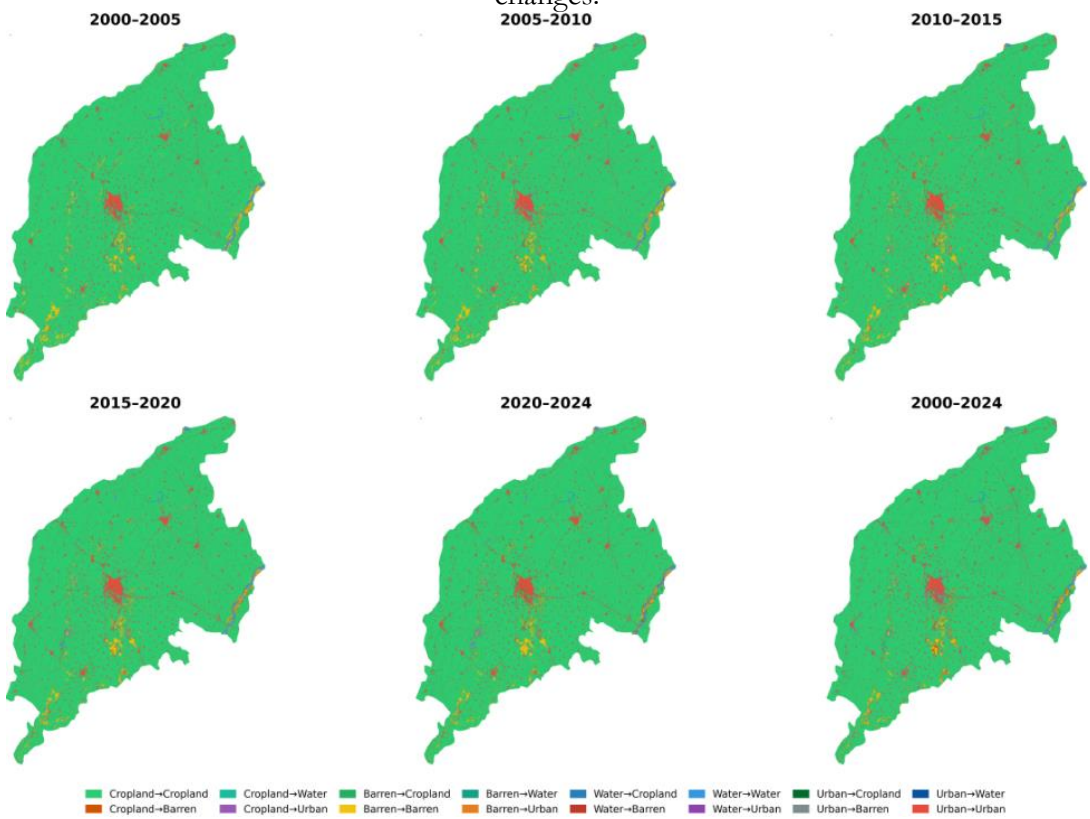


Figure 6. Spatiotemporal LULC transition maps of Sargodha District for six-time intervals showing class-to-class conversions.

The transition maps indicate that much of the landscape maintained its cropland identity during the observation period, while change was concentrated around pre-existing built-up cores (Figure 6). The maps indicate a progressive outward pattern around Sargodha City and smaller, more dispersed changes in the direction of Bhalwal and Shahpur. This distribution suggests that urban development was spatially selective rather than uniformly scattered across the agricultural plain. The largest net period of development, 2010-2015, is also mapped as having a more conspicuous peri-urban change footprint.

Taken together, the spatial maps, area statistics and transition visualizations describe an evolving agro-urban mosaic. Cropland continued to account for over nine-tenths of the mapped district in 2024, but it lost area across every analyzed interval. Urban growth was persistent and most intense in the middle of the series. The changed pixels were associated with established settlements and their surroundings, while the majority of the district retained a predominantly agricultural land-cover pattern.

Discussion:

Urbanization in a Predominantly Agricultural Landscape:

The strongest conclusion from the evidence is that a measurable increase in constructed land occurred within a landscape that remained overwhelmingly agricultural. The built-up class increased by 101.70 km² between 2000 and 2024. Although 35.04% growth represents a substantial relative expansion of the initial urban class, the associated change in district-wide cover was 1.755 percentage points. Both expressions are useful. Relative growth communicates the scale of change in the urban footprint; percentage-point growth shows that cropland retained its district-wide dominance. This dual perspective helps avoid presenting gradual conversion as either negligible or a wholesale replacement of agriculture. Findings from studies of Lahore, Multan, Khanewal and Khairpur provide context for the relationship between urban land growth and competing land uses [6][7][8][9][10]. They consistently motivate attention to agricultural conversion, although their study areas, classification categories and reporting periods differ. Direct numerical comparisons are therefore potentially misleading. The Sargodha results make a complementary contribution by demonstrating that the competing demands of urban land and cropland also matter in a district where the built-up share was still below 7% in 2024. Urban planning pressure is not confined to highly urbanized metropolitan regions.

The timing is noteworthy. The 2010-2015 period supplied 39.69 km², or 39.03%, of the total reported net urban gain. A five-year interval with such a large share point to a temporally concentrated phase of development, although it does not independently identify the policy decision, road project, migration process or investment responsible. Residential growth, infrastructure investment and demographic pressure have been proposed as potential drivers. These explanations are plausible and broadly consistent with research on settlement expansion [2][4][9], but their relative contributions were not statistically evaluated. Establishing causation would require geocoded approvals, road-opening dates, built-up permits or temporally aligned socioeconomic series.

Agricultural Conversion and the Interpretation of Class Change:

The net cropland reduction of 79.34 km² deserves attention even though it represents only 1.49% of the original mapped cropland extent. The position of newly built-up areas around urban centres creates the possibility of land fragmentation and land-price pressure on adjoining agricultural parcels. However, this investigation does not quantify changes in farm size, crop yield or household income. The present results should therefore be interpreted as evidence of mapped cropland contraction rather than as a measured decrease in agricultural production or food security. Similar caution has been urged in environmental analyses where a land-cover indicator is used as a proxy for a more complex social or ecological outcome [3][7][12][31]. The decline in barren land complicates a simple narrative of one-way agricultural

loss. Exposed soil may be recultivated, left fallow, converted to built-up land or differently classified between seasonal images. Consequently, the observation that barren land lost 22.19 km² does not establish a definite area of land reclamation. Conversely, a barren-to-cropland transition in a thematic comparison is informative but would be strengthened by field-based agricultural history or multi-season imagery. This is especially important in irrigated plains where land preparation can create temporary bare-soil signatures and where 30 m pixels may contain combinations of soil, crops and structures [13][20][21].

Spatial conversion maps are thus valuable but should be treated as the beginning of interpretation, not its conclusion. For development control, locations repeatedly flagged as cropland-to-built-up could be prioritized for higher-resolution verification, field inspection and comparison with land-use permissions. This produces a practical monitoring strategy without assuming that every isolated change pixel records genuine construction. Established methodological guidance also recommends reporting area-adjusted change estimates and confidence intervals based on independent reference samples before drawing strong conclusions about small differences [22][32].

Methodological Strengths and Limitations:

An important strength of the multi-date dataset is its six-date temporal structure. A comparison of 2000 and 2024 alone would conceal the pronounced 2010-2015 expansion phase and the lower 2015-2020 gain. The same four LULC categories are used across all periods and can be compared directly in area tables. RF classification incorporates multiple spectral bands and indices, while class-specific error metrics provide more information than a single headline OA. Together, these elements provide a useful baseline for district-level land monitoring [19][20][33][34]. The evidence also has constraints that should remain visible in any journal article. First, Landsat's 30 m pixels cannot reliably resolve all narrow roads, minor structures, crop boundaries or small canals. Second, the processing records contain unresolved differences in the listed sensor–year assignments and software, and no complete acquisition log or RF hyperparameter record is provided. Third, the reported 2023-2024 field observations do not in themselves demonstrate independent historical reference labels for all six epochs. Fourth, despite reasonable overall agreement, mapped transitions have not been assigned their own uncertainty estimates. Fifth, class areas sum to 5,794.49 km² rather than the approximate 5,864 km² district area stated in the study description. These points affect reproducibility and the precision of change interpretation. They are disclosed rather than resolved by inventing missing information. Other limitations are interpretive. An urban spectral class is not equivalent to a legal urban boundary, and a cropland class does not measure harvest, income or irrigation reliability. Similarly, the slight net variation in mapped water is not a hydrological stability test. The study does not contain sufficient evidence to infer a rate of groundwater depletion, impervious-surface runoff changes or urban heat-island intensification. Those issues are reasonable directions for subsequent research, given previous work on environmental consequences of urban expansion in Pakistan [7][23][35][36][37], but they are not findings of this article.

Implications for Land-use Monitoring and Planning:

The results justify targeted attention to the interface between settlement expansion and cultivation. Sargodha City and its surrounding agricultural fringe represent a practical monitoring priority, followed by the growing built-up zones around Bhalwal and Shahpur identified in the change maps. An operational programme could repeat comparable land-cover classification at regular intervals, screen possible cropland-to-built-up pixels, verify priority sites with higher-resolution imagery and compare observed conversions with planning permissions. This would convert a retrospective geospatial study into a continuing spatial evidence base for district planners.

A second implication is that land-balance reporting should separate net class changes from gross transitions. Net expansion is relevant to district statistics, but gross cropland-to-urban conversion is the more direct indicator of agricultural land consumed by new infrastructure. Future monitoring should therefore archive the classified maps, provide their transition matrices, retain independent date-specific reference samples and report uncertainty for conversion totals. Published recommendations for land-change accuracy and area estimation provide a defensible framework for this improvement [22][32]. A third priority is transparent documentation of image dates, sensor processing, reference sampling and classifier settings so that a subsequent analyst can reproduce the results without relying on narrative descriptions alone [1][26][33]. These actions are consistent with urban-growth management and agricultural zoning, but the present study does not assess the legal feasibility or economic outcomes of individual policies. It offers a spatially grounded diagnostic: where developed land has expanded, when the fastest increase occurred and how much cropland has declined in net terms. Decisions about containment zones, protection of productive fields or expansion of services would require consultation with the local planning and agricultural departments, particularly where map boundaries overlap with existing settlements or disputed land records [11].

Conclusion:

Six Landsat-based classifications show persistent built-up expansion in Sargodha District between 2000 and 2024, within a landscape that remained dominated by cropland. Urban area increased from 290.22 to 391.92 km², a net gain of 101.70 km² (35.04%). Cropland declined from 5,319.22 to 5,239.88 km², a net loss of 79.34 km². The largest five-year urban gain occurred in 2010-2015 (39.69 km²). Spatial comparisons locate conspicuous change around Sargodha City and other developed centres. Barren land declined by 22.19 km², while the net mapped water change was -0.17 km². The map accuracies were reported between 89.00% and 95.95%. The focused finding is an expanding agro-urban interface, not the disappearance of Sargodha's agricultural landscape. This pattern supports regular monitoring of the urban fringe and closer review of cropland conversion in land-use planning. The numerical totals provide a baseline, while the unresolved mapped-area discrepancy, incomplete historic validation information and absence of change-specific uncertainty should be addressed before the results are used as precision estimates of agricultural land consumption. No future scenario or causal model has been inferred from these descriptive observations.

Publication and Submission Declaration:

The authors confirm that this manuscript has not been published previously and is not under consideration by another journal.

Acknowledgment:

The authors acknowledge the United States Geological Survey for providing the public earthquake catalogue used in this study.

Funding:

This research received no external funding.

Conflict of Interest:

The authors declare no conflict of interest.

Author Contributions:

All authors made significant contributions to the conceptualization, methodology, data analysis, software development, validation, and interpretation of the study. The authors collectively contributed to manuscript preparation, review, and editing. All authors have read, approved, and agreed with the content of the final manuscript and accept accountability for all aspects of the work.

References:

[1] M. A. Wulder, J. G. Masek, W. B. Cohen, T. R. Loveland, and C. E. Woodcock,

"Opening the archive: How free data has enabled the science and monitoring promise of Landsat," *Remote Sens. Environ.*, vol. 122, pp. 2–10, Jul. 2012, doi: 10.1016/J.RSE.2012.01.010.

[2] K. C. Seto, B. Güneralp, and L. R. Hutyra, "Global forecasts of urban expansion to 2030 and direct impacts on biodiversity and carbon pools," *Proc. Natl. Acad. Sci.*, vol. 109, no. 40, pp. 16083–16088, Oct. 2012, doi: 10.1073/PNAS.1211658109.

[3] R. L. B. Hooke, J. F. Martín-Duque, and J. Pedraza, "Land transformation by humans: A review," *GSA Today*, vol. 22, no. 12, pp. 4–10, Dec. 2012, doi: 10.1130/GSAT151A.1.

[4] T. V. Ha, M. Tuohy, M. Irwin, and P. V. Tuan, "Monitoring and mapping rural urbanization and land use changes using Landsat data in the northeast subtropical region of Vietnam," *Egypt. J. Remote Sens. Sp. Sci.*, vol. 23, no. 1, pp. 11–19, Apr. 2020, doi: 10.1016/J.EJRS.2018.07.001.

[5] M. Z. Iqbal and M. J. Iqbal, "Land Use Detection Using Remote Sensing and GIS (A Case Study of Rawalpindi Division)," *Am. J. Remote Sens. 2018, Vol. 6, Page 39*, vol. 6, no. 1, pp. 39–51, Apr. 2018, doi: 10.11648/J.AJRS.20180601.17.

[6] S. Hussain and S. Karuppannan, "Land use/land cover changes and their impact on land surface temperature using remote sensing technique in district Khanewal, Punjab Pakistan," *Geol. Ecol. Landscapes*, 2021, doi: 10.1080/24749508.2021.1923272.

[7] Z. Tahir, M. Haseeb, S. A. Mahmood, N. E. Hassan, M. M. Dogar, and S. Z. Hassan, "From Green to Grey: Assessing the Impact of Urbanization on Land Surface Temperature and Thermal Comfort in Multan City," *Earth Syst. Environ. 2025 92*, vol. 9, no. 2, pp. 777–800, Feb. 2025, doi: 10.1007/S41748-025-00598-Y.

[8] M. Hashim* *et al.*, "Application of Geospatial Approaches for Evaluation of Urban Growth Pattern and Trend Prediction of Multan City, Pakistan," *Int. J. Innov. Sci. Technol.*, vol. 7, no. 9, pp. 108–120, 2025, Accessed: Aug. 31, 2026. [Online]. Available: https://ideas.repec.org/a/abq/ijist1/v7y2025i9p108-120.html

[9] M. Sarwar, S. Mahmood, and W. Habib, "Assessing Urban Expansion and Land Cover Change in City District Lahore using Multi-Stage Satellite Data," *Int. J. Innov. Sci. Technol.*, vol. 7, no. 9, pp. 94–107, 2025, Accessed: Nov. 05, 2026. [Online]. Available: https://ideas.repec.org/a/abq/ijist1/v7y2025i9p94-107.html

[10] A. A. Maitlo, N. H. Chandio, K. Hussain*, S. Mal, N. Noor, and M. WaseemNoonari, "Impact of Urbanization on Land Use and Land Cover: A Geospatial investigation of Taluka Khairpur (2000-2020)," *Int. J. Innov. Sci. Technol.*, vol. 7, no. 9, pp. 77–84, 2025, Accessed: Nov. 05, 2026. [Online]. Available: https://ideas.repec.org/a/abq/ijist1/v7y2025i9p77-84.html

[11] Z. Tahir *et al.*, "Predicting land use and land cover changes for sustainable land management using CA-Markov modelling and GIS techniques," *Sci. Rep.*, vol. 15, no. 1, Dec. 2025, doi: 10.1038/S41598-025-87796-W.

[12] G. N. Vivekananda, R. Swathi, and A. V. L. N. Sujith, "Multi-temporal image analysis for LULC classification and change detection," *Eur. J. Remote Sens.*, vol. 54, no. sup2, pp. 189–199, 2021, doi: 10.1080/22797254.2020.1771215.

[13] C. Liping, S. Yujun, and S. Saeed, "Monitoring and predicting land use and land cover changes using remote sensing and GIS techniques—A case study of a hilly area, Jiangle, China," *PLoS One*, vol. 13, no. 7, p. e0200493, Jul. 2018, doi: 10.1371/JOURNAL.PONE.0200493.

[14] M. M. H. Seyam, M. R. Haque, and M. M. Rahman, "Identifying the land use land cover (LULC) changes using remote sensing and GIS approach: A case study at Bhaluka in Mymensingh, Bangladesh," *Case Stud. Chem. Environ. Eng.*, vol. 7, p. 100293, Jun. 2023, doi: 10.1016/J.CSCEE.2022.100293.

[15] U. Bayarsaikhan, B. Boldgiv, K. R. Kim, K. A. Park, and D. Lee, "Change detection and classification of land cover at Hustai National Park in Mongolia," *Int. J. Appl. Earth Obs. Geoinf.*, vol. 11, no. 4, pp. 273–280, Aug. 2009, doi: 10.1016/J.JAG.2009.03.004.

[16] Giles M. Foody, "Status of land cover classification accuracy assessment," *Remote Sens. Environ.*, vol. 80, no. 1, pp. 185–201, 2002, doi: https://doi.org/10.1016/S0034-4257(01)00295-4.

[17] Y. Sreedhar, A. Nagaraju, and G. Murali Krishna, "An Appraisal of Land Use/Land Cover Change Scenario of Tummalapalle, Cuddapah Region, India—A Remote Sensing and GIS Perspective," *Adv. Remote Sens.*, vol. 05, no. 04, pp. 232–245, 2016, doi: 10.4236/ARS.2016.54019.

[18] R. G. Congalton, "A review of assessing the accuracy of classifications of remotely sensed data," *Remote Sens. Environ.*, vol. 37, no. 1, pp. 35–46, Jul. 1991, doi: 10.1016/0034-4257(91)90048-B.

[19] L. Breiman, "Random forests," *Mach. Learn.*, vol. 45, no. 1, pp. 5–32, Oct. 2001, doi: 10.1023/A:1010933404324.

[20] R. Sonobe, Y. Yamaya, H. Tani, X. Wang, N. Kobayashi, and K. Mochizuki, "Crop classification from Sentinel-2-derived vegetation indices using ensemble learning," *J. Appl. Remote Sens.*, vol. 12, no. 02, pp. 1–16, May 2018, doi: 10.1117/1.JRS.12.026019.

[21] H. Hoppe *et al.*, "Transferability of Machine Learning Models for Crop Classification in Remote Sensing Imagery Using a New Test Methodology: A Study on Phenological, Temporal, and Spatial Influences," *Remote Sens. 2024, Vol. 16, Page 1493*, vol. 16, no. 9, p. 1493, Apr. 2024, doi: 10.3390/RS16091493.

[22] P. Olofsson, G. M.Foodu, H. Martin, V. S. Stephen, E. W. Curtis, and M. A. Wuldwe, *Good practices for estimating area and assessing accuracy of land change*, vol. 148. 2013.

[23] M. Nasar-u-Minallah, D. Haase, S. Qureshi, S. Zia, and M. Fatima, "Ecological monitoring of urban thermal field variance index and determining the surface urban heat island effects in Lahore, Pakistan," *Environ. Monit. Assess. 2023 19510*, vol. 195, no. 10, pp. 1212-, Sep. 2023, doi: 10.1007/S10661-023-11799-1.

[24] Z. Hao *et al.*, "Multitemporal Analysis of Urbanization-Driven Slope and Ecological Impact Using Machine-Learning and Remote Sensing Techniques," *IEEE J. Sel. Top. Appl. Earth Obs. Remote Sens.*, vol. 18, pp. 1876–1895, 2025, doi: 10.1109/JSTARS.2024.3509133.

[25] M. Zhao *et al.*, "Mapping urban dynamics (1992–2018) in Southeast Asia using consistent nighttime light data from DMSP and VIIRS," *Remote Sens. Environ.*, vol. 248, Oct. 2020, doi: 10.1016/J.RSE.2020.111980.

[26] N. Gorelick, M. Hancher, M. Dixon, S. Ilyushchenko, D. Thau, and R. Moore, "Google Earth Engine: Planetary-scale geospatial analysis for everyone," *Remote Sens. Environ.*, vol. 202, pp. 18–27, Dec. 2017, doi: 10.1016/J.RSE.2017.06.031.

[27] Y. Zha, J. Gao, and S. Ni, "Use of normalized difference built-up index in automatically mapping urban areas from TM imagery," *Int. J. Remote Sens.*, vol. 24, no. 3, pp. 583–594, Feb. 2003, doi: 10.1080/01431160304987.

[28] H. Xu, "Modification of normalised difference water index (NDWI) to enhance open water features in remotely sensed imagery," *Int. J. Remote Sens.*, vol. 27, no. 14, pp. 3025–3033, Jul. 2006, doi: 10.1080/01431160600589179.

[29] R. G. Pontius and M. Millones, "Death to Kappa: birth of quantity disagreement and allocation disagreement for accuracy assessment," *Int. J. Remote Sens.*, vol. 32, no. 15, pp. 4407–4429, 2011, doi: 10.1080/01431161.2011.552923.

[30] P. K. Srivastava, D. Han, M. A. Rico-Ramirez, M. Bray, and T. Islam, "Selection of classification techniques for land use/land cover change investigation," *Adv. Sp. Res.*,

vol. 50, no. 9, pp. 1250–1265, Nov. 2012, doi: 10.1016/J.ASR.2012.06.032.

[31] M. Haseeb, Z. Tahir, S. A. Mahmood, S. Batool, and M. U. Farooq, "Spatial soil loss prediction impacted by long-term land use/land cover change: a case study of Swat District," *Environ. Monit. Assess. 2023 1961*, vol. 196, no. 1, pp. 37-, Dec. 2023, doi: 10.1007/S10661-023-12200-X.

[32] P. Olofsson, G. M. Foody, S. V. Stehman, and C. E. Woodcock, "Making better use of accuracy data in land change studies: Estimating accuracy and area and quantifying uncertainty using stratified estimation," *Remote Sens. Environ.*, vol. 129, pp. 122–131, Feb. 2013, doi: 10.1016/J.RSE.2012.10.031.

[33] H. Zhang, M. Gao, and C. Ren, "Feature-Ensemble-Based Crop Mapping for Multi-Temporal Sentinel-2 Data Using Oversampling Algorithms and Gray Wolf Optimizer Support Vector Machine," *Remote Sens. 2022, Vol. 14, Page 5259*, vol. 14, no. 20, p. 5259, Oct. 2022, doi: 10.3390/RS14205259.

[34] R. Tufail, P. Tassinari, and D. Torreggiani, "Assessing feature extraction, selection, and classification combinations for crop mapping using Sentinel-2 time series: A case study in northern Italy," *Remote Sens. Appl. Soc. Environ.*, vol. 38, p. 101525, Apr. 2025, doi: 10.1016/J.RSASE.2025.101525.

[35] I. Khan *et al.*, "Impact assessment of land use change on surface temperature and agricultural productivity in Peshawar-Pakistan," *Environ. Sci. Pollut. Res.*, vol. 26, no. 32, pp. 33076–33085, Nov. 2019, doi: 10.1007/S11356-019-06448-5/METRICS.

[36] C. S. Chanu, L. Elango, and G. R. Shankar, "A geospatial approach for assessing the relation between changing land use/land cover and environmental parameters including land surface temperature of Chennai metropolitan city, India," *Arab. J. Geosci. 2021 142*, vol. 14, no. 2, pp. 132-, Jan. 2021, doi: 10.1007/S12517-020-06409-0.

[37] R. Khan *et al.*, "Monitoring land use land cover changes and its impacts on land surface temperature over Mardan and Charsadda Districts, Khyber Pakhtunkhwa (KP), Pakistan," *Environ. Monit. Assess. 2022 1946*, vol. 194, no. 6, pp. 409-, May 2022, doi: 10.1007/S10661-022-10072-1.



Copyright © by authors and 50Sea. This work is licensed under Creative Commons Attribution 4.0 International License.